In-plane thermal diffusivity estimation by radial fin method

Thomas Pierre, Edouard Geslain, Mickael Courtois, Anthony Magueresse, Thibaut Colinart

Version of Record: https://www.sciencedirect.com/science/article/pii/S1350449521003704
Manuscript_840eda6cf199089b8300520efd5a9e29

In-plane thermal diffusivity estimation by radial fin method

Abstract

This work presents a methodology to estimate the in-plane thermal diffusivity through infrared thermography. Experimentally, a vertical thin-thickness sample is briefly heated on its center by Joule effect and one face is filmed by an infrared camera. The experimental temperature field is compared with an analytical axisymmetric semi-infinite thermal model. The in-plane thermal diffusivity and a modified Biot number are estimated through a least square method based on the minimization of the quadratic error between the experimental and the theoretical temperatures. The methodology is applied to four samples with a broad range of thermal conductivity: balsa, PVC, mild steel, and aluminum alloy. The analysis of the residuals and of the parameter correlation coefficients show the feasibility of the method for isotropic materials for which a rather good agreement with literature data is found. When applied to anisotropic materials like balsa, the method shows the possibility with one experiment to characterize in every material directions.

Nomenclature

Latine letters

e	thickness, m
c_p^m	specific heat, J·kg^{-1}·K^{-1}
G	transmittance
h	heat exchange coefficient, W·m^{-2}·K^{-1}
H	modified Biot number, m^{-2}

I modified Bessel function

k thermal conductivity, $W \cdot m^{-1} \cdot K^{-1}$

K modified Bessel function

l length, m

N measurements number

r radial coordinate, m

R radius, m

s Laplace parameter, s^{-1}

t time, s

T temperature, K

x position, m

Greek letters

α thermal diffusivity, $m^2 \cdot s^{-1}$

ζ parameter

θ temperature, K

ρ density, $kg \cdot m^{-3}$

σ standard-deviation

τ heating time, s

φ flux density, $W \cdot m^{-2}$

Φ flux density, $W \cdot m^{-2}$

χ reduced sensitivity

Indices and subscripts

0 initial

∞ infinity

exp experimental

est estimated

min minimum

1. Introduction

This work deals with the estimation of the in-plane thermal diffusivity of isotropic and anisotropic materials. This property is of interest in many topics since numerous parametric publications concern, for example, its evolution versus the ageing [1], the porosity of thermal barrier coatings [2], the nature of composites [3] or thin films [4]. Many devices and methodologies exist to characterize anisotropic materials. Therefore, we limit this bibliography to techniques using both experiments and multidimensional analytical models.

Initially proposed by Parker et al. [5] to estimate the in-depth thermal diffusivity, the flash method ([6-11] for example) is now considered as a standard methodology: a brief heat flux is applied in the sample thickness direction and the temperature along the cross section (front or rear face) is measured and compared with the one given by a theoretical model. The main uncertainties with the non-contact heating remain the precise knowledge of the spatial energy distribution and of the absorbed part of this energy received by the surface. Nowadays the systematic use of infrared camera avoids the uncertainties due to the location of the temperature sensors such as the thermocouple, and "provides a great number of data to evaluate the variance of the estimated parameters by statistical methods" [10]. For thermal heating with contact, for example with a hot-rod [12], the major uncertainty is the difference between the real surface contact and the geometrical one of the heating element.

The classic shape of non-contact heating is the Gaussian spot [2,6,11-13], but others studies proposed these schemes: annular area [4], line or strip [10], grid-like mask [8], or uneven [7]. Considering the Gaussian shape heating, derivative methods provide successful results for isotropic and anisotropic materials, using multidimensional models: the Gaussian shape temperature fitting method [9,12], the logarithmic parabolas method [13], the lock-in thermography [14,15], the pulsed phase thermography [16], or the flying spot method [17,18].

The great majority of the theoretical studies are based on flux/temperature models, meaning that the flux is the input and the temperature the observable. This type of approach is dependent of additional unknowns, such as the convective and radiative heat losses. To circumvent this problem, and therefore diminish the number of unknown parameters, temperature/temperature models are relevant [19,20]. For example, from works of Hadisaroyo et al. [7] and Philippi et al. [10], Remy et al. [21] worked on this approach with isotropic sample of glass. Experimentally, the sample is heated by uneven laser flash and an infrared camera films the longitudinal propagation of the heat along the surface. The knowledge of the heat flux is not necessary anymore, since the theoretical 1D model expresses the linear relation between the temperature at a position x functions of two temperatures at positions x_1 and x_2 on both sides of x. The in-plane thermal diffusivity and the heat losses by fin effect are estimated successfully, since they are uncorrelated. Recently, Jannot et al. [22] diminished the number of input temperatures, since they adapted the previous model to semi-infinite isotropic sample.

In the view of estimating in-plane thermal diffusivity of isotropic materials and, also, of anisotropic materials, we propose in this study to use a temperature-temperature 1D semi-infinite model in the cylindrical coordinates and to develop the corresponding experimental set-up by paying attention to the heating source. In this view, thermal model

is presented in Section 2, while the estimation procedure of two unknown parameters (in-plane thermal diffusivity and a modified Biot number) is discussed in Section 3. The new experimental set-up is introduced in Section 4. The results obtained on materials with thermal conductivity ranging between 10^{-1} and 10^{2} W.m^{-1}.K^{-1} are presented and discussed in Section 5.

2. Theoretical models

Figure 1 presents a view of a thin thickness semi-infinite medium (cylinder of radius $R \to \infty$) with isotropic thermal diffusivity α and heat capacity ρc_p^m. Temperature is initially uniform and a heat flow rate (here, a crenel shape of duration τ) is applied on its center. The heat equation in the sample and its initial and boundary conditions are represented by the system (1) assuming a monodimensional fin model. T is the modified temperature once removed T_∞ the environment temperature, e is the sample thickness, k the thermal conductivity, h the heat exchange coefficient, and $\varphi_0(t)$ the flux density at the position r_0. By solving the system (1), the temperature variations $T(r,t)$ can be evaluated for any positions. Here, two approaches are considered: temperature is deduced either from the flux density (flux-temperature semi-infinite model) or from another temperature (temperature-temperature semi-infinite model).

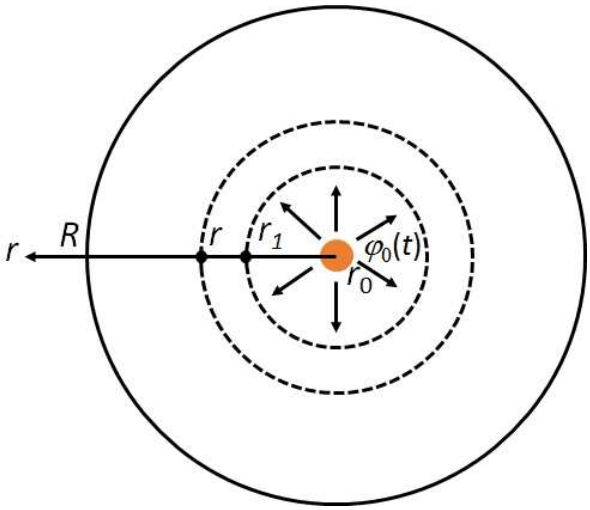

Figure 1. Sketch of the theoretical model for semi-finite medium.

$$\frac{\partial^2 T}{\partial r^2} + \frac{1}{r}\frac{\partial T}{\partial r} - \frac{2h(R+e)}{keR}T = \frac{1}{\alpha}\frac{\partial T}{\partial t} \tag{1a}$$

$$T(r,0) = 0 \tag{1b}$$

$$-k\frac{\partial T(r_0,t)}{\partial r} = \varphi_0(t) \tag{1c}$$

$$T(\infty,t) \to 0 \tag{1d}$$

2.1. Flux-temperature semi-infinite model

After a Laplace transform of parameter s according to the time (2) where $f(r,t)$ can either be the temperature $T(r,t)$ or the flux $\varphi_0(t)$, the solution of the system (1) is given by the relations (3) expressing the temperature in the Laplace domain along the radius r. The use of a relevant numerical inverse Laplace algorithm [23] allows to get the temperature as function of time. The flux-temperature semi-infinite model (3) has been validated by comparison with simulations through ComsolMultiphysics® for different positions along the radius (not presented here).

$$F(r,s) = \int_0^{\infty} f(r,t)e^{-st}dt \tag{2}$$

$$\theta(r,s) = \frac{\Phi_0(s)}{k\omega}\frac{K_0(\omega r)}{K_1(\omega r_0)} \tag{3a}$$

$$\omega = \sqrt{\frac{s}{\alpha} + H} \tag{3b}$$

$$H \approx \frac{2h}{ke} \tag{3c}$$

2.2. Temperature-temperature semi-infinite model

The quadrupole formalism [24] is very convenient to simply express the temperature along the r-direction between two coordinates r_1 and r (4):

$$\begin{bmatrix}\theta(r_1,s)\\ \Phi(r_1,s)\end{bmatrix} = \begin{bmatrix}A & B\\ C & D\end{bmatrix}\begin{bmatrix}\theta(r,s)\\ \Phi(r,s)\end{bmatrix} \tag{4a}$$

$$A = \omega r[K_1(\omega r)I_0(\omega r_1) + K_0(\omega r_1)I_1(\omega r)] \tag{4b}$$

$$B = \frac{1}{2\pi kl}[I_0(\omega r)K_0(\omega r_1) - I_0(\omega r_1)K_0(\omega r)] \tag{4c}$$

$$C = 2\pi kl\omega^2 r_1 r[K_1(\omega r_1)I_1(\omega r) - K_1(\omega r)I_1(\omega r_1)] \tag{4d}$$

$$D = \omega r_1[K_1(\omega r_1)I_0(\omega r) + K_0(\omega r)I_1(\omega r_1)] \tag{4e}$$

where I_0, I_1, K_0, and K_1 are the modified Bessel functions. In the time domain, temperature at radius r is given as function temperature at radius r_1 as:

$$T(r,t) = T(r_1,t) \otimes L^{-1}[G(s)] \tag{5a}$$

$$G(s) = \frac{K_0(\omega r)}{K_0(\omega r_1)} \tag{5b}$$

where r and r_1 are the two coordinates and L^{-1} the inverse Laplace transform. The function G depends on two parameters: the in-plane thermal diffusivity α and the modified Biot number H (3c).

Figures 2a and 2b compare temperatures at radius r predicted by the flux-temperature semi-infinite models (3) and temperature-temperature semi-infinite models (5) for balsa and aluminum, respectively. Thermal properties are taken from literature or from laboratory measurements (Table 2). The heat exchange coefficient h is set to 10 $W \cdot m^{-2} \cdot K^{-1}$, and $\tau = 6$ s and 1 s, for the balsa and aluminum, respectively. A good agreement is found between both models. Note however that it is not always the case due to the choice of both the initial time t_0 (which must be non-null since $s = 1/t$) and of the time step δt needed in the inverse Laplace algorithm. In the present case, $t_0 = 10$ ms and $\delta t = 10$ ms.

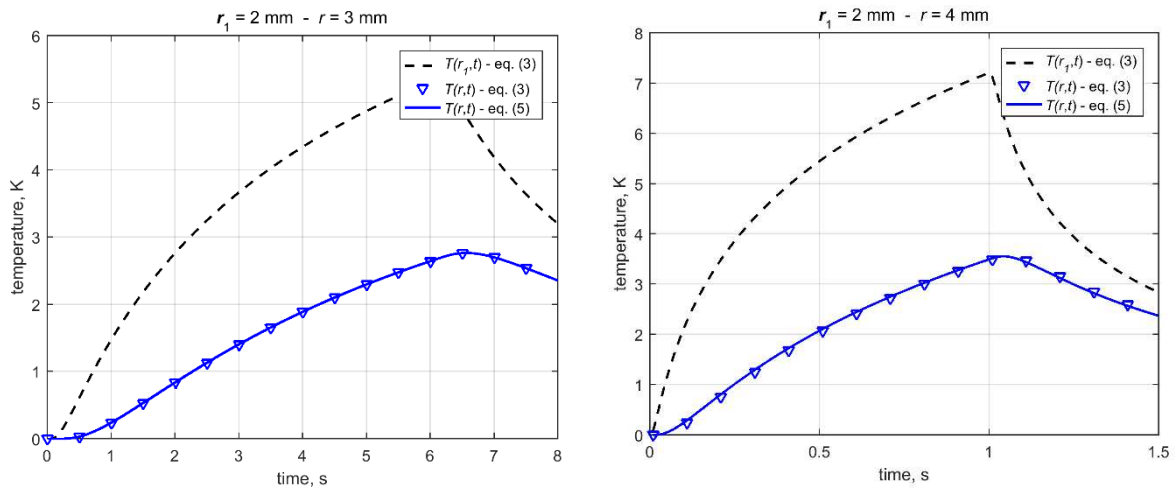

Figure 2. Comparison of temperature evolutions predicted by flux-temperature and temperature-temperature semi-infinite models for balsa (a) and aluminum (b).

3. Sensitivity study and choice of the two positions

Two experimental temperatures are required to perform an estimation with the relation (5): the observable $T^{exp}(r,t)$ and the input temperature $T^{exp}(r_1,t)$. The estimation consists in minimizing the quadratic error between the experimental and the theoretical temperatures at the position r by ordinary least squares coupled with a Levenberg-Marquardt algorithm [25,26] (6-7). In relation (7), $\sigma$is the standard deviation of the experimental noise and $N$the number of measurements.

$$T^{est}(r,t) = T^{exp}(r_1,t) \otimes L^{-1}[G_1(s)] \tag{6}$$

$$\sum_{i=1}^{N} |T^{exp}(r,t) - T^{est}(r,t)|^2 \rightarrow N\sigma^2 \tag{7}$$

There are two parameters to estimate: the in-plane thermal diffusivity α and the modified Biot number H. It is convenient to perform a sensitivity study to evaluate the feasibility of estimation and the correlation level between them by quantifying a correlation coefficient.

The reduced sensitivity χ_ζ (8) allows to express the sensitivity of the transfer function $G(s)$ versus the parameter ζ.

$$\chi_\zeta = \zeta \frac{\partial L^{-1}[G(s)]}{\partial \zeta} \tag{8}$$

This reduced sensitivity χ_ζ is adimensioned, therefore, once convoluted by $T^{exp}(r_1,t)$, χ_ζ has the unit of the temperature and allows to compare its amplitude regarding the noise level during experiment. Theoretical plots representing the reduced sensitivities χ_ζ are presented in the case of the balsa and the aluminum in Figures 3a and 3b, respectively.

Both figures show different behaviors between the sensitivity to the in-plane thermal diffusivity and to the modified Biot number, which allows to predict that the estimation of both parameters seems possible. In Figure 3a, for the balsa, the sensitivity to the modified Biot number H decreases slowly, but in Figure 3b, the transfer function seems to be insensitive to H in the case of the aluminum, which presumes that its estimation would be difficult.

The correlation coefficient $\sigma_{\alpha H}^2$ defines the correlation level between both parameters. "Parameters tend not to be correlated when $\sigma_{\alpha H}^2$ tends to 0, and on the contrary become more and more correlated when $\sigma_{\alpha H}^2$ tends to $\pm$ 1" [27]. This parameter is studied versus the two positions r_1 and r, which are not as random as expected. Here is presented the case of the choice of the position r, and more precisely the distance $r - r_1$. The case of the sole position r_1 is discussed in section 4. In Figure 3a, for the balsa and $r - r_1 = 1$ mm, $\sigma_{\alpha H}^2 =$ -0.245 and in Figure 3b for the aluminum and $r - r_1 = 2$ mm, $\sigma_{\alpha H}^2 =$ 0.192. Figure 4 shows for the balsa and the aluminum the theoretical evolution of $\sigma_{\alpha H}^2$ versus the distance $r - r_1$. It happens that the former has a minimum value, corresponding to the minimum correlation between the in-plane thermal diffusivity and the modified Biot number. This evolution will be systematically studied during the parameter estimation versus $r - r_1$.

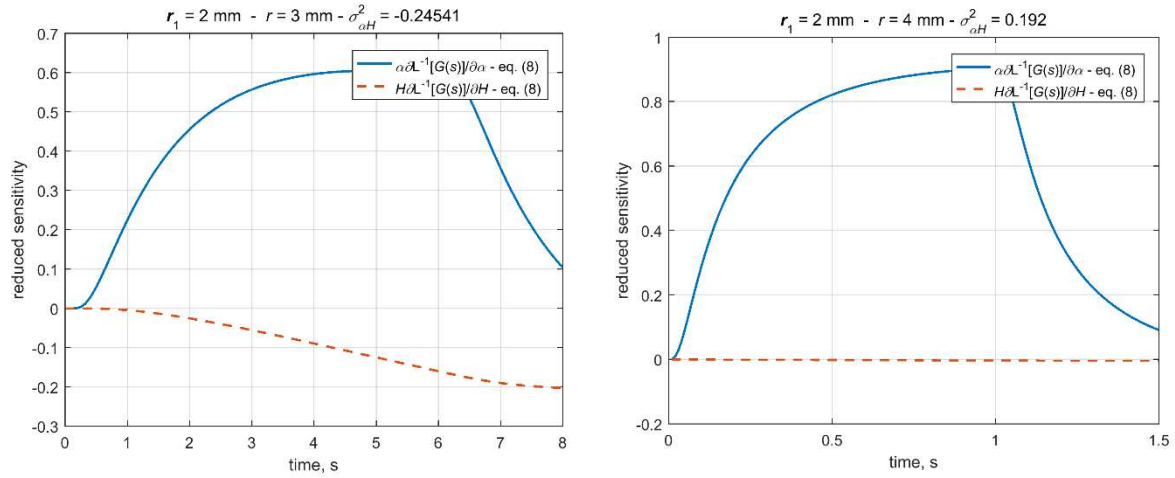

Figure 3. Reduced sensitivity curves to α and H in the cases of the balsa (a) and of the aluminum (b).

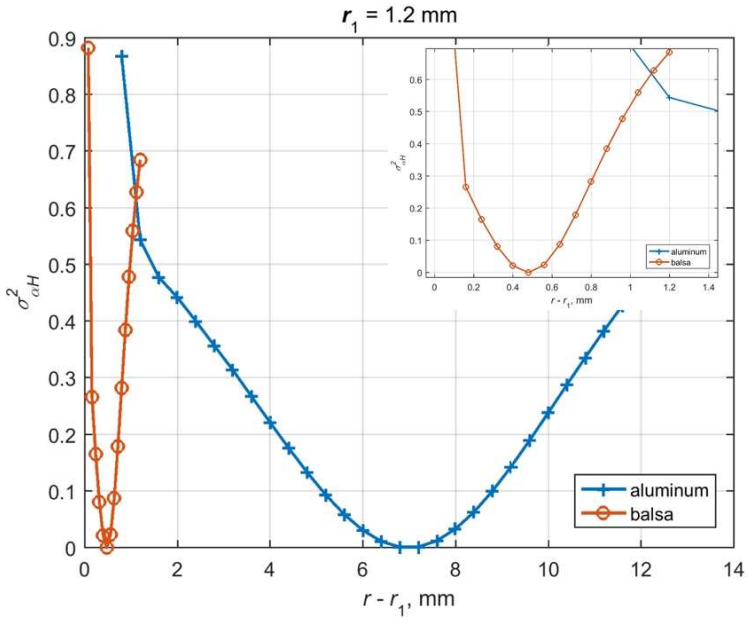

Figure 4. Comparison between the evolution of the correlation $\sigma^2_{\alpha H}$ coefficient for balsa and aluminum.

4. Materials and methods

An experimental set-up presented in Figures 5 and 6 is developed to correspond to the theoretical model. A thin sample is heated on its center by a heating source. This heating source must be designed to really have a thermal heating in the radial direction, such as imposed in the thermal model (1c). Here, the heating source is a cylindrical copper spot of about $r_0 = 1$ mm radius embedded in the sample (to avoid any thermal contact resistance) and heated by Joule effect through electric current coming from the sample rear face. The electric wires are maintained with conductive stick, which should be let dry at least for 24h. The heat flux is imposed during few seconds and stopped when a maximum temperature increase of 10 °C is reached in the sample or when the semi-infinite assumption is not valid anymore.

The temperature of the sample front face is measured during the experiment with a high sensitivity ($<$ 25 mK) infrared camera FLIR X6580sc equipped with a G1 microscopic high distance objective. It films a scene of 9.60×7.68 mm^2 with a resolution of 15 µm (InSb detector of 640×512 pixels) and a frequency of 10 Hz ($\delta t = 100$ ms). Since the sample temperature increase is lower than 10 °C, the evolution of the radiative flux versus the temperature is assumed linear whatever the emissivity value. The contact resistance between the copper spot and the sample is not evaluated, nevertheless Figure 7 shows an example of infrared scene measured for mild steel. One observes a good temperature homogeneity of the copper spot, no overheating between the spot and the sample indicating a good thermal contact and an isotropic surface temperature decrease of the sample.

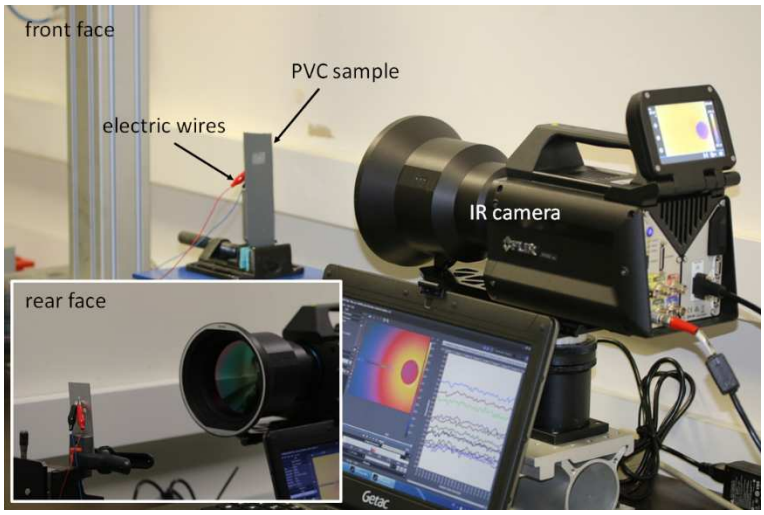

Figure 5. View of the experimental set-up.

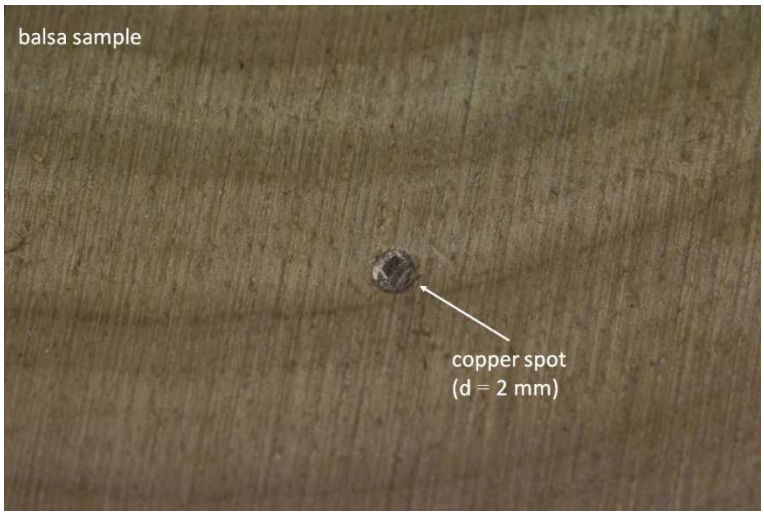

Figure 6. View of the copper spot embedded in the balsa sample.

Every infrared scenes at each time step are recorded and then analyzed with the help of a Matlab® program. As shown in Figure 7 and according to Figure 1, the position $r = 0$ is the center of the copper spot and is defined through the position (x_0, y_0) in the infrared scene. Therefore it is easy to know the location of a temperature $T(r,t)$ for some given r radius and θ angle, meaning the coordinates (x, y) , with relations (9) and (10). The temperature corresponds to the temperature of a sole pixel, implying possible weak

signal-to-noise ratio, especially during tests with the aluminum sample (see Section 5). The passage from pixel to distance is made possible thanks to the resolution (15 µm).

$$x = x_0 - rcos(\theta) \quad (9)$$

$$y = y_0 - rsin(\theta) \quad (10)$$

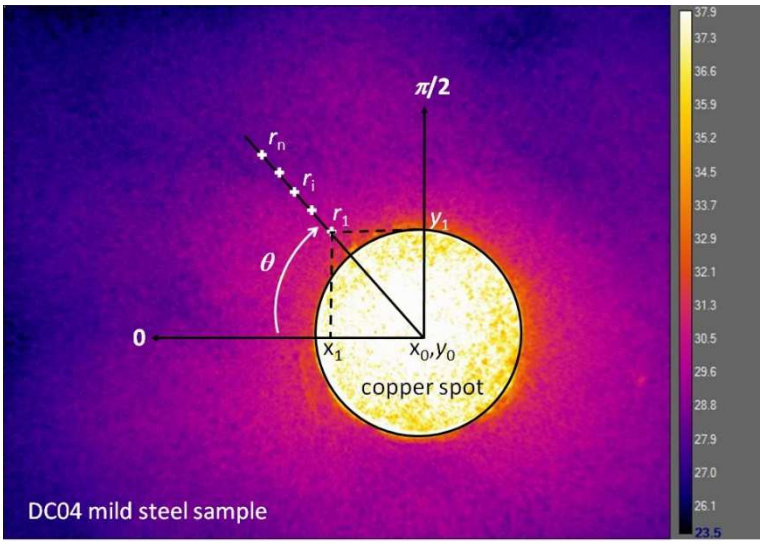

Figure 7. Representation of an infrared scene measured for mild steel and of the relation between the Cartesian and the polar coordinates. The scale on the right is temperature expressed in degrees Celsius.

Four samples of 2 mm thickness are tested, with thermal conductivities ranged approximately between 10^{-1} and 10^{2}, three isotropic ones: aluminum alloy (AA5182), mild steel (DC04), and PVC; and one anisotropic: balsa. The thermophysical properties gathered in Table 1 are either taken from the literature [28-30] or measured in lab with Laser Flash Apparatus (Netzsch LFA 457 MicroFlash®) or microcalorimeter (Setaram µsDc3 evo). Note that before performing the experiment, the aluminum alloy and mild steel samples have

been sandblasted to increase their emissivity in order to drastically reduce the influence of the environment. The experimental conditions are different from one sample to the other.

Table 1. Dimensions and thermal properties of the tested materials (* laboratory measurements).

	balsa		aluminum alloy AA5182	mild steel DC54 [29]	PVC [30]
	(//)	(⊥)			
k (Wm^{-1}·K^{-1})	0.105 ± 0.007 [28]	0.046 ± 0.007 [28]		66,1	0.250 ± 0.020
ρ (kg·m^{-3})	166 ± 3*			7 750	1 214 ± 10*
c_p^m (J·kg^{-1}·K^{-1})	1 036 ± 40*			446	1 014 ± 35*
α (mm^2·s^{-1})	0.95 ± 0.03	0.48 ± 0.02	53.65 ± 1.32*	19.12 18.70*	0.20 ± 0.03

5. Results and analysis

The results are presented first for the PVC (Section 5.1), then for the mild steel DC54 and the aluminum alloy AA5182 (Section 5.2), and finally for the balsa considering the orientation of its fibers (Section 5.3). Table 2 gathers all results at the end of this Section 5. The estimation results for α^{est} and H^{est} are given with an average value $\bar{\zeta}^{est}$ and its standard deviation σ_ζ.

5.1. Detailed analysis for PVC sample

The first sample is the PVC. For two given r_1 and r positions, and for different angles ranged between 0 and $\pi/2$ according to equations (9)-(10), Figure 8 presents experimental temperatures of roughly same evolutions versus time. They are almost independent of the angle, confirming therefore the isotropic nature of PVC. Tests with mild steel and aluminum alloy present similar observations. Next, all the parameter estimations are performed from the temperature measured at the angle 0°.

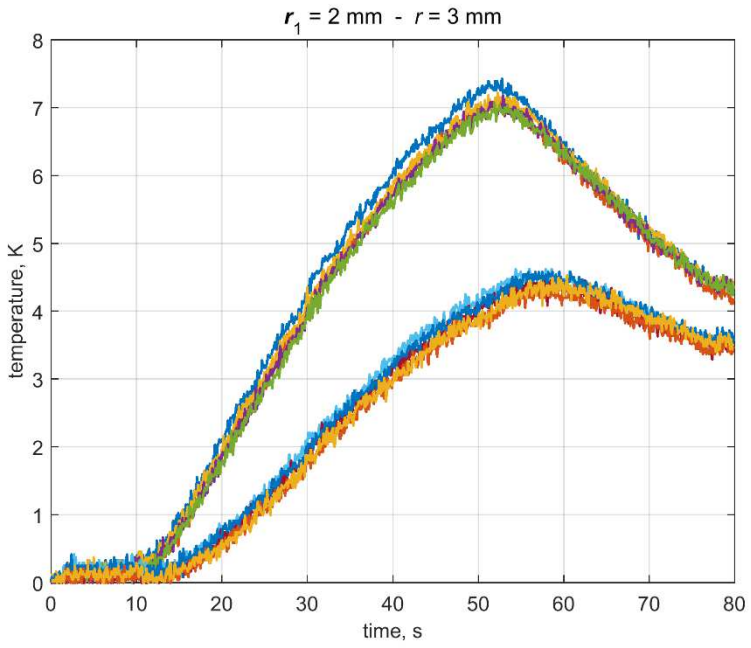

Figure 8. Experimental temperature variations of PVC for angles $\theta = 0$, $\pi/6$, $\pi/4$, $\pi/3$, $\pi/2$ and for $r_1 = 2$ mm (the highest) and $r = 3$ mm.

Then the estimation method presented in Section 3 is used. Figure 9 presents the correlation coefficient $\sigma^2_{\alpha H}$ as function of the distance $r - r_1$ for $r_1 = 2$ mm and r varying until the maximum distance filmed by the infrared camera ($r_1 - r = 3$ mm), which varies with the experiments. Figure 9 is rather similar to Figure 4 with a minimum for $r - r_1 = 0.7$ mm. It shows that for $r - r_1 < 0.70$ mm, the covariance varies to large extend with values close to 1: the fitting of the theoretical model on the experimental temperature is unsuccessful and the estimated values have no meaning. For $r - r_1 > 0.70$ mm, the covariance increases slightly from 0.45 to 0.7 and the theoretical model fits on the experimental temperatures: large possibilities exist to estimate the properties.

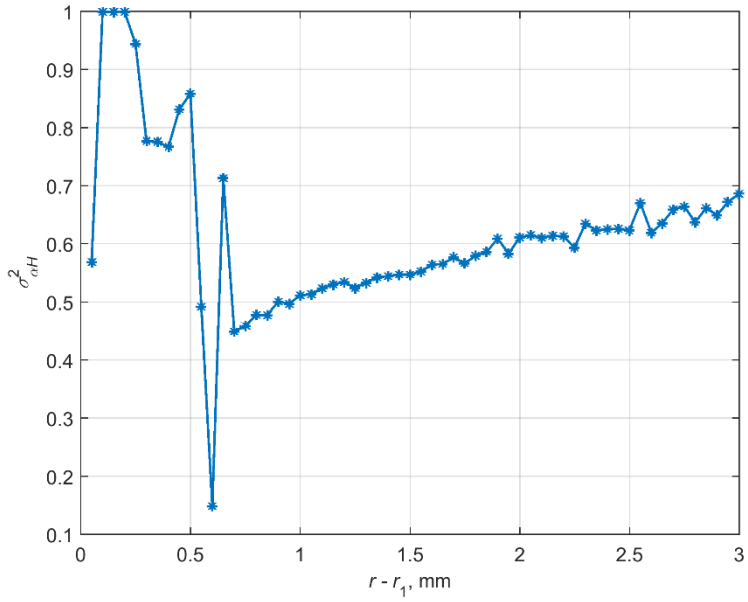

Figure 9. Evolution of the variance $\sigma^2_{\alpha H}$ versus the distance $r - r_1$ for $\theta = 0$ and $r_1 = 2$ mm.

An example of temperature estimation during test with PVC for $\theta = 0$ is presented in Figure 10, for the given position $r_1 = 2$ mm and $r_1 - r = 0.7$ mm when the covariance $\sigma^2_{\alpha H}$ starts to have a low value (see Figure 9). The residuals seem to be constantly around the zero value.

The estimation is extended for several positions r_1. For a given r_1, position r is searched to reach the minimum of $\sigma^2_{\alpha H}$ over the distance $r - r1$ and, then, estimated parameters are recorded.

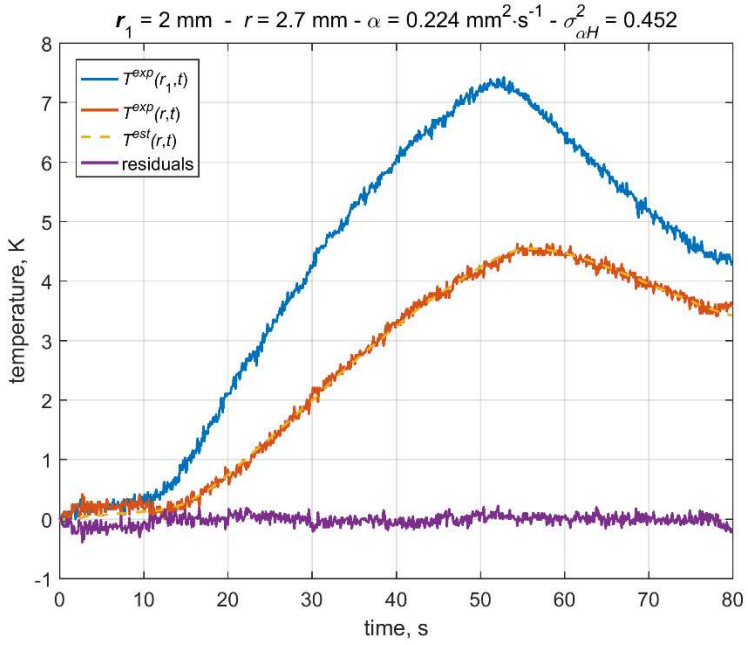

Figure 10. Experimental and estimated temperatures during test with PVC.

The statistical distribution of the estimated parameters are plotted in Figures 11 and 12. In-plane thermal diffusivity α can be roughly fitted with a Gaussian law. For the mean value is equal to 0.221 mm^2.s^{-1} and similar to the reference (see Table 2). Regarding the modified Biot number H, the distribution is more uniform and scattered, which may be due to the low sensitivity of this parameter (see Figures 3). Nevertheless, from the thermal conductivity value of the PVC found in the literature, the calculation of the heat exchange coefficient h gives a value coherent with the free convection [30].

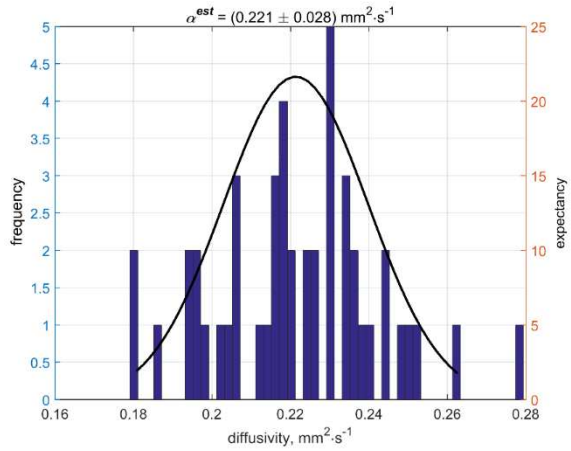

Figure 11. Statistical distribution of the estimated in-plane thermal diffusivity of PVC.

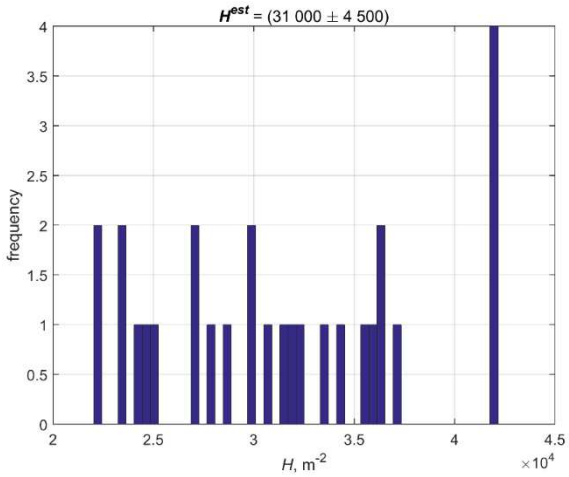

Figure 12. Statistical distribution of the estimated modified Biot number for PVC.

5.2. Results for metallic samples

The detailed analysis performed for the PVC is repeated for the metallic samples, the DC54 mild steel and the AA5182 aluminum alloy, where the isotropic behavior is confirmed.

Figures 13 and 14 present the statistical distribution of estimated in-plane thermal diffusivity for the DC54 mild steel, and the AA5182 aluminum alloy. The in-plane thermal diffusivity estimation seems consistent with literature. However the dispersion is important (particularly for the aluminum alloy).

A temperature-temperature model for a finite medium, presented in Appendix A, has also been developed and tested, but it does not improve the estimation. There is no more sensitivity with the additional temperature at the position r_2.

Because of the high in-plane thermal diffusivity of metallic samples and the limited power supply, the temperature increase could not be above 3 °C for the aluminum alloy (instead of 10 °C). On the one side, this makes the choice of the position r_1 more difficult.

On the other side, the modified Biot number H cannot be estimated, since the observable is insensitive to it (as shown in Figure 3). The tests with the aluminum shows one limitation of the techniques considering the current size of the sample. A solution to improve the quality of the measurement and thus reduce the great dispersion would be to work with larger sample and supply a more important electric power to reach the 10 °C and have a higher signal-to-noise ratio.

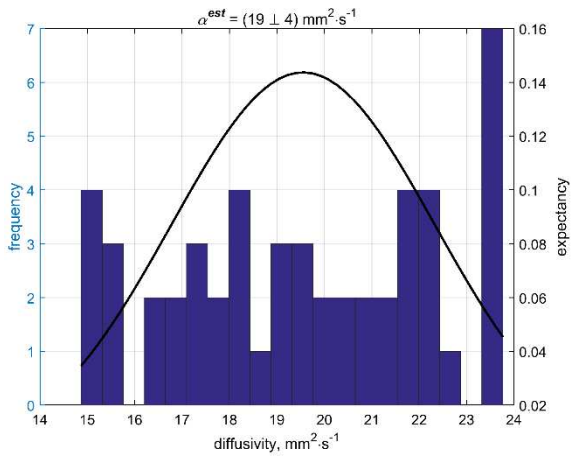

Figure 13. Statistical distribution of the estimated in-plane thermal diffusivity values of DC54 mild steel.

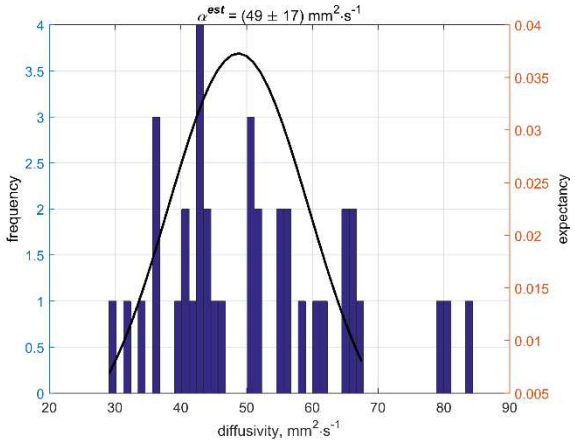

Figure 14. Statistical distribution of the estimated in-plane thermal diffusivity values of AA5182 aluminum alloy.

5.3. Results for anisotropic sample

In this last section, the analysis is performed for balsa, which is anisotropic due to its biological structure. Figure 15 shows an infrared scene during sample heating. Copper spot appears cooler than the surrounding due to its low emissivity compared with balsa one. Temperature distribution is not homogeneous on balsa surface, highlighting the anisotropic structure of the material. Here, the heat flux tends to flow preferentially in the vertical direction ($\theta = \pi/2$ in Figure 15), along the longitudinal direction (e.g. natural

orientation of the fibers (//)). Therefore the transverse direction (⊥) is defined for $\theta = 0$. The analysis is performed in these two main directions.

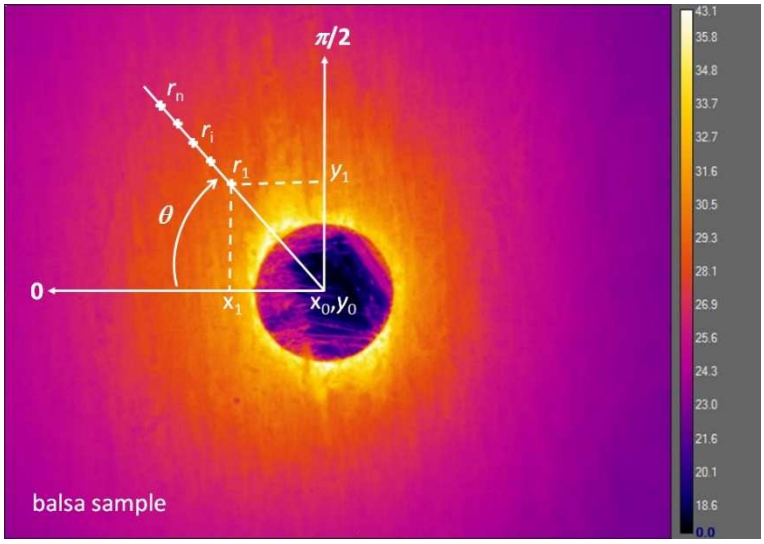

Figure 15. Infrared scene of the balsa with fibers oriented in the vertical direction ($\theta = \pi/2$). The scale on the right is temperature expressed in degrees Celsius.

Figures 16 and 17 shows the statistical distribution for in-plane thermal diffusivities in longitudinal and transverse direction. Except some points, all results are centered on a single value with a rather important standard deviation. The mean values have the same order of magnitude than literature data [28]. Nevertheless, it is slightly lower in the longitudinal direction and higher in the transverse direction. Therefore, the thermal diffusivity ratio between both directions is only 1.3, compared to the ratio of 2.2 measured by the guarded hot-plate technique [31]. On the other hand, the modified Biot number H ratio is equal to 2.5 assuming an identical heat exchange coefficient in both directions.

The choice of the r_1 position is experimental and can vary from one sample to the other. Of course, it must be placed after r_0, meaning beyond the radius of the copper spot,

but not too close to avoid some possible effects of the contact resistance between the copper spot and the sample.

As reported in Table 2, the heat exchange coefficient h expressed in relation (4b) is consistent with free convection values considering the estimated values of H and the thermal conductivity k of the samples found in the literature. Besides, the real Biot number ($he/2k$) is calculated to verify the fin effect assumption (see Section 2). A value of $h = 10$ W·m^{-2}·K^{-1} is considered for the aluminum and the mild steel. Except for the measurements with the balsa with $\theta = 0°$, where $Bi = 0.09 \pm 0.06$, meaning close to the limit value of 0.1, the fin effect assumption is always verified.

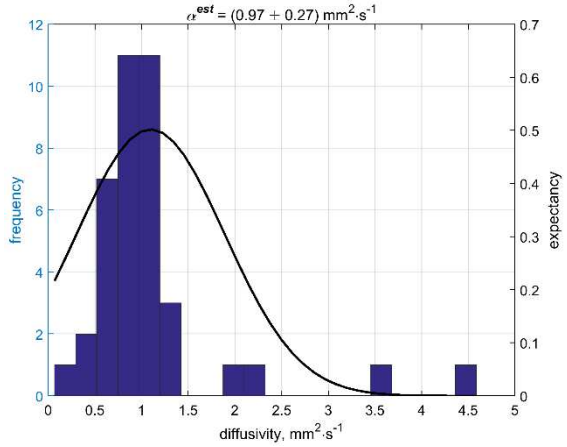

Figure 16. Statistical distribution of the estimated transverse in-plane thermal diffusivity of balsa (⊥).

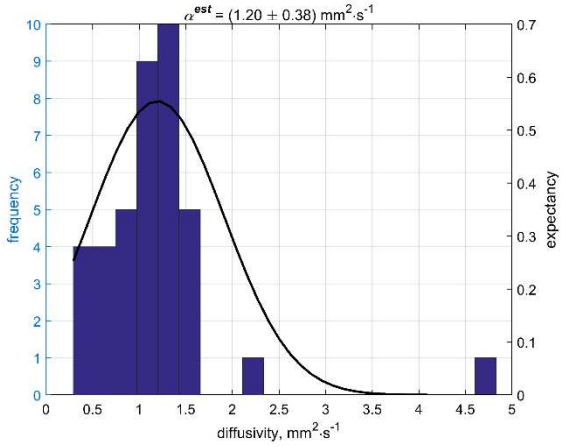

Figure 17. Statistical distribution of the estimated longitudinal in-plane thermal diffusivity of balsa (//).

Table 2. Estimation results for the four samples (* interpolated value from laboratory measurements, ** for $h = 10$ W·m^{-2}·K^{-1}).

	balsa ⊥	balsa //	PVC	DC54	AA5182
r_1	2.00	2.00	2.00	2.00	2.00

(mm)					
r_{min} (mm)	3.15	3.10	3.15	4.65	6.00
$\alpha^{est} \pm \sigma_\alpha$ ($mm^2 \cdot s^{-1}$)	0.97 ± 0.27	1.20 ± 0.38	0.22 ± 0.03	19 ± 4	49 ± 17
α literature ($mm^2 \cdot s^{-1}$)	0.48 ± 0.02	0.95 ± 0.03	0.20 ± 0.03	18.70*	$53.6^* \pm 1.4^*$
$H_{est} \pm \sigma_H$ ($10^3\ m^{-2}$)	90 ± 30	21.5 ± 6.9	31.0 ± 4.5	-	-
h ($W \cdot m^{-2} \cdot K^{-1}$)	4.1 ± 2.1	4.5 ± 1.9	7.8 ± 2.0	-	-
$Bi = he/2k$	0.09 ± 0.06	0.02 ± 0.03	0.03 ± 0.02	$< 10^{-3}$**	$< 10^{-3}$**

Conclusion

This work presented an analytical temperature-temperature model dedicated to the estimation of the in-plane thermal diffusivity for isotropic and anisotropic materials. Its feasibility has been proved for materials of thermal conductivity ranged between 10^{-1} and 10^2 $W \cdot m^{-1} \cdot K^{-1}$. From an existing method in Cartesian coordinates, the present one is adapted in the cylindrical ones considering the fin effect and the semi-infinite assumption. This theoretical model expresses the temperature at a position r (observable) functions of an imposed temperature at a position r_1 (input data) convoluted by a transfer function (transmittance) depending on the in-plane thermal diffusivity and of a modified Biot number. Experimentally, the heating is assured by Joule effect in the radial direction through an embedded copper spot (contrary to the major cases in the literature where the heating is performed by laser in the thickness direction) and the temperatures are

measured by an infrared camera. A sensitivity study showed that both parameters could be estimated accurately, and the estimation was performed by least squares by the minimization of the quadratic error between the experimental and the theoretical temperatures. Classically, the quality of the estimation is confronted with information given by inverse method algorithms such as the parameters correlation coefficients and the residuals. The choice of the positions r_1 and r must also be considered with care. The position r_1 changes from one sample to the other, due to the possible influence of the contact resistance between the sample and the copper spot. Whatever r_1, it appears that the distance $r - r_1$, for a given sample, corresponding to the minimum value of correlation coefficient $\sigma_{\alpha H}^2$ is approximately the same. However, the displacement of r_1 away from r_0, and thus of r makes the estimation less accurate due to the sensitivity decrease. In this study, three isotropic materials were first tested, successfully for the PVC and the mild steel, but with large uncertainties for the aluminum, making appear the limitation of the method due to the combination of a high conductive material, a sample of too small dimensions, and a power supply too limitative. However, the average estimation results are coherent with those found in the literature. An anisotropic balsa sample was finally tested, and the in-plane thermal diffusivity estimated according to two directions: parallel and orthogonal to the natural directions of the fibers. Results are consistent with literature but rather high, and the influence of the fiber orientation was showed. Even if parameter estimation was performed for two directions, the data post-treatment procedure, presented in Section 4, allows to work in any direction with only one experiment, therefore making possible to realize an in-plane thermal diffusivity map of the sample.

It was obvious that some temperatures were rather noisy, whatever the sample. This is due to the G1 microscopic objective of the infrared camera, where each pixel aims

an area of 15 × 15 µm². Compared with the size of a thermocouple probe of about 200 µm, the signal measured by the infrared camera is more submitted to noise. Therefore it will be necessary to work with temperature signals of more than one pixel by taking into account the others around.

Finally, only room temperature materials have been tested, however it seems that there is no limitation to extend this methodology to materials at higher temperature, implying a modification of the theoretical model.

Appendix A – Flux-temperature and temperature-temperature models in finite medium

Figure 18 and equations (1a)-(1c), and (A.1) present the theoretical model in the case of a finite material, and its description is the same as presented in section 2.1.

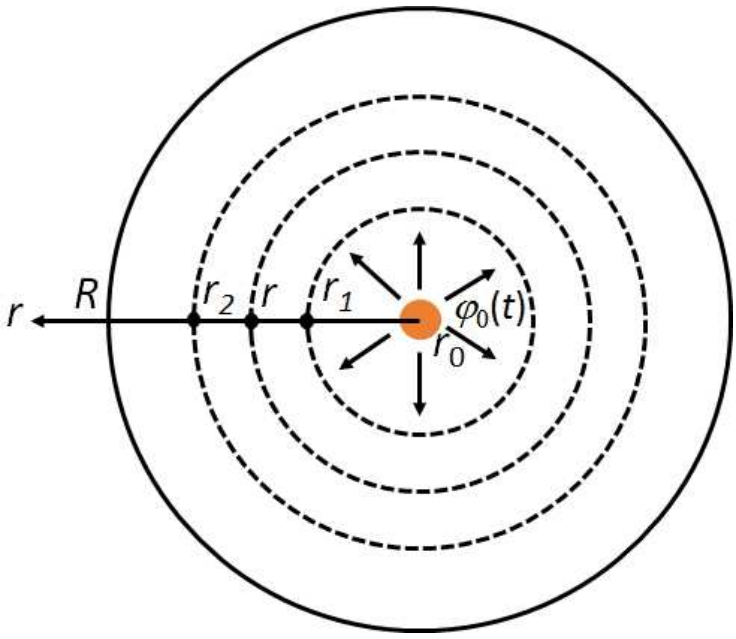

Figure 18. Sketch of the theoretical model for finite medium.

$$T(R,t) = 0 \qquad \text{(A.1)}$$

After a Laplace transform of parameter s according to the time (2), the solution of the system (A.1) is given by the relations (A.2) expressing the temperature in the Laplace domain along the radius r.

$$\theta(r,s) = \frac{\Phi_0(s)}{k\omega} \frac{I_0(\omega r)K_0(\omega R) + I_0(\omega R)K_0(\omega r)}{I_1(\omega r_0)K_0(\omega R) + I_0(\omega R)K_1(\omega r_0)} \tag{A.2a}$$

$$H = \frac{2h(R+e)}{keR} \tag{A.2b}$$

According to the same system (4), it is possible to express a temperature-temperature model expressing the temperature $T(r,t)$ in a random position r knowing the temperatures $T(r_1,t)$ and $T(r_2,t)$ at two positions r_1 and r_2 on both sides, each of these temperatures being convoluted by a transfer function (transmittance) in the cylindrical coordinates:

$$T(r,t) = T(r_1,t) \otimes L^{-1}[G_1(s)] + T(r_2,t) \otimes L^{-1}[G_2(s)] \tag{A.3a}$$

$$G_1(s) = \frac{I_0(\omega r)K_0(\omega r_2) - I_0(\omega r_2)K_0(\omega r)}{I_0(\omega r_1)K_0(\omega r_2) - I_0(\omega r_2)K_0(\omega r_1)} \tag{A.3b}$$

$$G_2(s) = \frac{I_0(\omega r_1)K_0(\omega r) - I_0(\omega r)K_0(\omega r_1)}{I_0(\omega r_1)K_0(\omega r_2) - I_0(\omega r_2)K_0(\omega r_1)} \tag{A.3c}$$

where r, r_1, and r_2 are the three coordinates and L^{-1} the inverse Laplace transform. The function G_1 and G_2 are functions of two parameters: the in-plane thermal diffusivity α and the modified Biot number H (A.3c). The system (A.3) shows explicitly that $T(r,t) = T(r_1,t)$ for $r = r_1$ and $T(r,t) = T(r_2,t)$ for $r = r_2$. Figure19 presents a comparison between all the finite and semi-infinite models proposed in the case of an aluminum sample. The

transmittances G_1, G_2, and G are also plotted in Figure 20. One can observe that G (semi-infinite model) is very close to G_1 (finite model).

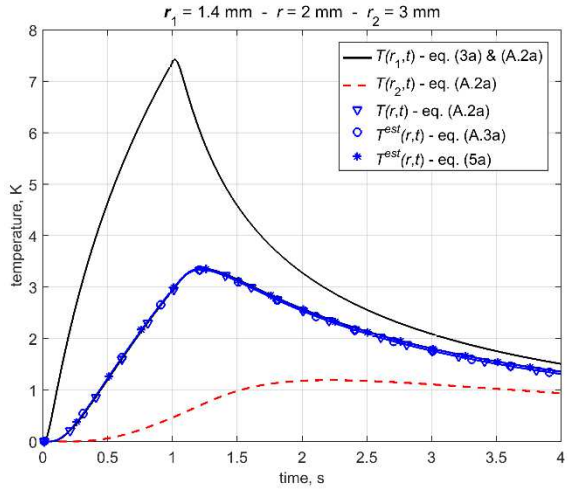

Figure 19. Comparison of the different temperatures model using the aluminum properties in finite and semi-infinite media.

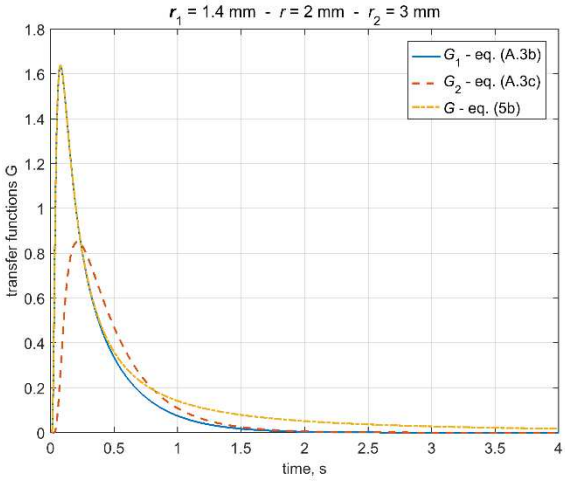

Figure 20. Evolution of the three transmittances in finite and semi-infinite media in the case of aluminum.

The finite and the semi-infinite models present the same results. However, as the semi-infinite model is functions of two positions instead of three for the finite one, the former has been preferred in this work to be used versus experimental data.

References

[1] P. Bison et al. « In-Depth and In-Plane Thermal Diffusivity Measurements of Thermal Barrier Coatings by IR Camera: Evaluation of Ageing ». *International Journal of Thermophysics*, vol. 29, nº 6, December 2008, p. 2149-61.

[2] P. Bison et al. « A Thermographic Technique for the Simultaneous Estimation of In-Plane and in-Depth Thermal Diffusivities of TBCs ». *Surface and Coatings Technology*, vol. 205, nº 10, February 2011, p. 3128-33.

[3] M. Bamford et al. « Global and Local Characterization of the Thermal Diffusivities of SiCf/SiC Composites with Infrared Thermography and Flash Method ». *Composites Science and Technology*, vol. 69, nº 7, June 2009, p. 1131-41.

[4] J. Gembarovic et al. « In-plane thermal diffusivity measurement of highly thermal conductive thin films by the flash method ». *2018 34th Thermal Measurement, Modeling Management Symposium (SEMI-THERM)*, 2018, p. 197-99.

[5] Parker, W. J., et al. « Flash Method of Determining Thermal Diffusivity, Heat Capacity, and Thermal Conductivity ». *Journal of Applied Physics*, vol. 32, nº 9, septembre 1961, p. 1679-84.

[6] W. Adamcyck et al., « Nondestructive, Real Time Technique for in-Plane Heat Diffusivity Measurements ». *International Journal of Heat and Mass Transfer*, vol. 154, juin 2020, p. 119659.

[7] D. Hadisaroyo et al. « Un appareillage simple pour la mesure de la diffusivité thermique de plaques minces ». *Journal de Physique III*, vol. 2, nº 1, janvier 1992, p. 111-28.

[8] J.-C. Krapez et al. « Measurement of In-Plane Diffusivity in Non-Homogeneous Slabs by Applying Flash Thermography ». *International Journal of Thermal Sciences*, vol. 43, nº 10, octobre 2004, p. 967-77.

[9] F. Cernuschi et al. « In-plane thermal diffusivity evaluation by infrared thermography ». *Review of Scientific Instruments*, vol. 72, nº 10, septembre 2001, p. 3988-95.

[10] I. Philippi et al. « Measurement of thermal diffusivities through processing of infrared images ». *Review of Scientific Instruments*, vol. 66, nº 1, janvier 1995, p. 182-92.

[11] N. W. Pech-May et al. « Simultaneous Measurement of the In-Plane and in-Depth Thermal Diffusivity of Solids Using Pulsed Infrared Thermography with Focused Illumination ». *NDT & E International*, vol. 77, janvier 2016, p. 28-34.

[12] C. M. Basheer et al. « Hot-Rod Thermography for in-Plane Thermal Diffusivity Measurement ». *Measurement*, vol. 103, juin 2017, p. 235-40.

[13] L. Gaverina et al. « Pulsed flying spot with the logarithmic parabolas method for the estimation of in-plane thermal diffusivity fields on heterogeneous and anisotropic materials ». *Journal of Applied Physics*, vol. 121, nº 11, mars 2017, p. 115105.

[14] Nolte, P. W., et al. « Thermal diffusivity of metals determined by lock-in thermography ». *Quantitative InfraRed Thermography Journal*, vol. 14, nº 2, juillet 2017, p. 218-25.

[15] A. Cifuentes et al. « Simultaneous Measurements of the Thermal Diffusivity and Conductivity of Thermal Insulators Using Lock-in Infrared Thermography ». *International Journal of Thermal Sciences*, vol. 121, novembre 2017, p. 305-12.

[16] Ospina-Borras, J. E., et al. « Thermal diffusivity estimation with quantitative pulsed phase thermography ». *Thermosense: Thermal Infrared Applications XXXVII*, vol. 9485, SPIE, 2015, p. 275-82.

[17] A. Salazar et al., *Laser-spot step-heating thermography to measure the thermal diffusivity of solids*, International Journal of Thermal Sciences 170 (2021) 107124.

[18] A. Bedoya et al. « Measurement of In-Plane Thermal Diffusivity of Solids Moving at Constant Velocity Using Laser Spot Infrared Thermography ». *Measurement*, vol. 134, février 2019, p. 519-26.

[19] Y. Jannot, A. Degiovanni, *Thermal properties measurements of materials*, ISTE Editions Ltd., London, 2018.

[20] Y. Jannot et al. « Thermal Conductivity Measurement of Insulating Materials with a Three Layers Device ». *International Journal of Heat and Mass Transfer*, vol. 52, n° 5, février 2009, p. 1105-11.

[21] B. Rémy, A. Degiovanni, D. Maillet, *Measurement of the in-plane thermal diffusivity of materials by infrared thermography*, International Journal of Thermophysics, Vol. 26, No. 2, March 2005.

[22] Y. Jannot et al. « In-plane thermal diffusivity measurement of thin plates by the transient fin method ». *Review of Scientific Instruments*, vol. 89, n° 10, octobre 2018, p. 104905.

[23] F. R. De Hoog, J. H. Knight, A. N. Stockes, *An improved method for numerical inversion of the Laplace transform*, SIAM J. Sci. Stat. Comput., Vol. 3, No. 3, 1982.

[24] D. Maillet, S. André, J.-C. Batsale, A. Degiovanni, C. Moyne, *Thermal quadrupoles, Solving the heat equation through integral transforms*, John Wiley & Sons, Ltd., New-York, 2000.

[25] H. Stehfest, *Algorithm 368, Numerical inversion and Laplace transforms*, Commun. ACM, 13, 47-49, 1970.

[26] H. Stehfest, *Remarks on* a*lgorithm 368, Numerical inversion and Laplace transforms*, Commun. ACM, 13, 624, 1970.

[27] F. Rigollet, D. Maillet, *Lecture 3. Basics for linear estimation, the white box case*, Metti 7 Advanced School, Thermal Measurements and Inverse Techniques, Volume 1: Lectures, Porquerolles, France, Sept. 29th – Oct. 4th, 2019.

[28] T. Pierre et al. « Transient infrared thermography to characterize thermal properties of millimeter-sized hemp shiv » *Quantitative Infrared Thermography Journal*, vol. 17, n°1, janvier 2020, p.63-77.

[29] E. Geslain, *Soudage par résistance des tôles fines revêtues : formation du noyau dans un assemblage de trois tôles*, thesis, Université Bretagne Sud, 2018.

[30] F. P. Incropera, *Fundamentals of Heat and Mass Transfer*. John Wiley & Sons, 2011.

[31] P. Carré, R. Le Gall, *Définition et détermination des conductivités thermiques dans les structures C.V.R. – balsa*, Rev. Gén. Therm. Fr., n°340, p. 211-215, avril 1990.